

Regional scale analysis of climate extremes in an SRM geoengineering simulation, Part 1: precipitation extremes

Rohi Muthyala^{1,2}, Govindasamy Bala^{1,*} and Aditya Nalam¹

¹Centre for Atmospheric and Oceanic Sciences, Indian Institute of Science, Bengaluru 560 012, India

²Present address: Department of Geography, Rutgers, The State University of New Jersey, Piscataway, NJ 08854, USA

In this study, we examine the statistics of precipitation extreme events in a model simulation of solar radiation management (SRM) geoengineering. We consider both intensity and frequency-based extreme indices for precipitation. The analysis is performed over both large-scale domains as well as regional scales (22 Giorgi land regions). We find that precipitation extremes are substantially reduced in geoengineering simulation: the magnitude of change is much smaller than those that occur in a simulation with elevated atmospheric CO₂ alone. In the geoengineered climate, though the global mean of the intensity of extreme precipitation events is slightly less than in control climate, substantial changes remain on regional scales. We do not find significant changes in the frequency of precipitation extremes in geoengineering simulation compared to control simulation on global and regional scales. We infer that SRM schemes are likely to reduce precipitation extremes and the associated impacts on a global scale. However, we note that a comprehensive assessment of moral, social, ethical, legal, technological, economic, political and governance issues is required for using SRM methods to counter the impacts of climate change.

Keywords: Geoengineering, solar radiation management, extreme events, regional analysis.

CLIMATE change is driven by changes in various external factors such as variation in solar radiation received by the earth, plate tectonics and volcanic eruptions. However, currently climate change caused by anthropogenic greenhouse gas (GHG) emissions is a major concern because much of the change in climate since the mid-20th century can be attributed to them¹. While reduction of emissions is the best way to reduce the impacts of climate change, alternative methods such as geoengineering have been proposed with an aim to deliberately alter the climate system on a large scale. The two major categories of geoengineering methods are solar radiation management (SRM) and carbon dioxide removal (CDR)²⁻⁷. SRM aims to counter the warming associated with increasing GHG concentrations by reducing the amount of sunlight absorbed by the climate system. CDR aims to slowdown

or perhaps reverse projected increases in the future atmospheric CO₂ concentrations by accelerating their natural removal and increasing the storage of carbon in land, ocean and geological reservoirs¹.

Previous modelling studies on SRM geoengineering⁸⁻¹⁷ show that geoengineering schemes can offset the changes in global mean surface temperature or global mean precipitation, but there could be large residual climate changes on regional scale. On a global scale, geoengineering would also lead to a weakened hydrological cycle¹⁸ if the global mean temperature changes are exactly offset. A GeoMIP (Geoengineering Model Intercomparison Project) study¹⁷ found that SRM in comparison to the pre-industrial climate, reduced precipitation and evaporation over land and especially in most monsoonal regions and in northern mid-latitudes and confirmed the weakening of hydrological cycle.

Climate change, driven by either natural or anthropogenic forcing, can lead to changes in the likelihood of occurrence or strength of extreme events¹. Since large sections of the society are most vulnerable to impacts of such events, a careful evaluation of future extreme events is needed. A robust characterization in terms of frequency and intensity is important, as planning of risk-reduction strategies requires reliable and detailed information on current and future climate extremes. This article is Part 1 of our two-part study on extremes under geoengineering: Part 1 is on precipitation extremes and Part 2 (ref. 19) discusses temperature extremes. In both the parts of this study, we separately discuss the intensity-based and frequency-based extreme indices.

Several modelling studies show that the intensity of extreme events is increasing under global warming²⁰⁻²⁸. For example, it has been shown that slight changes in the frequency distribution parameters can alter the precipitation extremes much more than the mean precipitation²⁰. Two possible mechanisms control both these short-term extreme precipitation amounts as well as changes in mean precipitation: thermodynamic and dynamic mechanisms²¹. Global warming increases the atmospheric water vapour content (thermodynamic mechanism) leading to changes in the hydrological cycle which include intensification of precipitation extremes. A multi-model study estimated

*For correspondence. (e-mail: gbala@iisc.ac.in)

that there will be an increase of about 6% per 1° warming in the globally averaged 20-year return values of annual extremes of daily precipitation amounts, with a bulk of the simulated values in the range 4–10% per 1° warming²⁴. However, global climate models (GCMs) are generally poor in simulating precipitation extremes and hence predicted that changes in a warmer climate vary among models²⁴. However, another study²⁹ showed that GCM predictions of extremes can be constrained by observed relationships in the present-day climate, it is found that extreme precipitation increases by 6–10% per °C of global mean surface warming.

Only a few studies in the past have investigated the statistics of extreme events under SRM geoengineering. Tilmes *et al.*¹⁷, using monthly output from multiple models (GeoMIP), quantified that the frequency of heavy precipitation events increases by 50% for a quadrupling of CO₂ in comparison to control conditions and reduces by 20% in geoengineering experiments. Using daily model output, Curry *et al.*³⁰ analysed the frequency of extreme events, such as coldest night, warmest day, maximum 5-days precipitation amount and a few duration indices. They showed that the climate extremes under geoengineering are not only smaller than 4XCO₂ conditions but also differ significantly from those under pre-industrial conditions. They also found that geoengineering is more effective in reducing changes in temperature extremes compared to precipitation extremes, and also reducing changes in precipitation extremes than means, but less effective in reducing changes in temperature extremes compared to means.

The major limitation in case of Tilmes *et al.*¹⁷ is that they use monthly mean precipitation data to evaluate the change in extreme precipitation intensity. Daily time resolution of the data is necessary to take into account the sub-monthly nature of extremes. Use of time-averaged data for analysing extremes will dampen their magnitude. Assessment of expected changes in surface temperature, precipitation and related extremes using daily output of the model was made by Curry *et al.*³⁰, but extreme events were defined using only a few ETCCDI (Expert Team of Climate Change Detection and Indices). Here, we perform an extensive assessment of the extremes using six precipitation extreme indices (three for intensity and three for frequency indices) and their projected changes in a geoengineered climate. We also quantify the changes in extremes over 22 Giorgi land regions and several large domains. Part 2 of this study discusses temperature extreme indices which are also distinctly classified into intensity-based and frequency-based indices¹⁹.

Model, experiments and methodology

Model details and experiments

The model used for this study is the NCAR (National Center for Atmospheric Research) global atmospheric

model, Community Atmosphere Model (CAM 5)³¹. It is coupled to the Community Land Model (CLM 4) and to a slab ocean model (SOM) with a thermodynamic sea-ice model to represent interactions with the ocean and sea-ice components of the climate system³². CAM 5 is the atmosphere component of the Community Earth System Model, version 1 (CESM1). We use horizontal resolution of the model of 1.9° in lat and 2.5° in long. There are 30 layers in the vertical covering 40 km.

In this study, three experiments are performed: (1) a pre-industrial control simulation ‘1XCO₂’ with a CO₂ concentration of 284.7 ppm and solar constant of 1367 Wm⁻²; (2) ‘2XCO₂’ with doubled atmospheric CO₂ concentration (i.e. 569.4 ppm), and solar constant of 1367 Wm⁻², (3) ‘Geo-Engg’ with doubled atmospheric CO₂ concentration (i.e. 569.4 ppm) and solar constant reduced by 2.25% (i.e. 1336.2 W m⁻²). All the experiments are run for 100 years and daily data from the last 10 years are used for analysis. These simulations take approximately 30 years to reach a near-equilibrium climate state. Since a decade is the minimum time-frame for meaningful assessments of climate change³³, our assessments of extremes use 10 years of daily data (91–100 years). We verified that the conclusions are not changed using another 10 year segment from the last 50 years daily output. We estimate from the 2XCO₂ case that for every 1°C of global mean surface temperature increase, global mean precipitation increases by 2%, in agreement with previous studies^{34–37}.

Observational data

Version 1.2 of the Global Precipitation Climatology Project (GPCP) one-degree daily combined precipitation dataset was used to evaluate the model simulated precipitation indices³⁸. This dataset is a first approach in estimating global daily precipitation at the 1° × 1° scale from observational data. It is composed of precipitation estimates from TMPI (Threshold Matched Precipitation Index) where available (40°N–40°S) and AdSND (adjusted sounding-based estimates from TIROS Operational Vertical Sounder and Atmospheric Infrared Sounder) elsewhere. We used 10 years (2004–2013) of GPCP data. As model data and observations are not at the same horizontal resolution, GPCP data were regridded (extrapolated) to model data resolution of 1.9° × 2.5°.

Methodology

Climate extremes are a multifaceted meteorological phenomenon and can be characterized in terms of intensity, frequency or duration of one or more climatological parameters²⁴. In this study, we considered a subset of precipitation indices available in EIA (ETCCDI Indices Archive). Even with identical amounts (i.e. means), the

Table 1. Set of extreme precipitation indices analysed in this study. These indices are recommended by the Expert Team of Climate Change Detection and Indices (ETCCDI), except those marked with an asterisk (*). The index marked with ** is defined by Sillmann *et al.*²⁷ to estimate the number of wet days

Label	Index	Index definition	Units
99.9p*	Extremely wet precipitation	The intensity of precipitation events which exceed 99.9th percentile threshold	mm/day
RX1day	Maximum 1 day precipitation	Maximum of daily precipitation amount	mm
RX5day	Maximum 5 days precipitation	Maximum of consecutive 5 days (cumulative) precipitation amount	mm
R1mm**	Number of wet days	Number of days with precipitation > 1 mm	days
R20mm	Very heavy precipitation days	Number of days with precipitation > 20 mm	days
R50mm*	Extreme precipitation days	Number of days with precipitation > 50 mm	days

climate can be different if the frequency and intensity of precipitation/temperature events differ³⁹. Therefore, we quantified the extreme precipitation events in terms of both intensity and frequency. As this study is based on a single model output, the control simulation (the 1XCO₂ case) thresholds were used as reference thresholds in estimating indices instead of a base observational threshold. Two new precipitation extreme indices, 99.9p and R50mm, were also used for a comprehensive assessment of extreme precipitation events. 99.9p represents the intensity of precipitation events which exceed 99.9th percentile threshold and R50mm is a frequency index, defined as the number of days with precipitation exceeding 50 mm. The selected indices (Table 1) give a comprehensive overview of changes in precipitation extremes in both 2XCO₂ and Geo-Engg cases^{27,28}. Regional extreme value statistics was performed for various selected regions ([Supplementary Table 1](#)) and for Giorgi land regions ([Supplementary Table 2](#) and [Supplementary Figure 1](#))⁴⁰. Spatial statistical analysis was also performed to estimate their uncertainties at local scale. Estimates for land and ocean regions were also made.

Methodology of estimating all precipitation extreme indices is not similar. We used two ways of aggregating individual events to create samples. The first method aggregates the events for the whole time-period (over the entire 10-year period in this study) for each grid point. Then precipitation extremes are estimated at each grid point based on their respective index definition and statistical analysis is performed over the spatial domain of interest. The second method, suitable for estimating zonal means of extremes, aggregates individual events over the 10-year period to estimate climate extreme events at each grid point and then averages along each latitude circle.

Results

Here we discuss the changes in precipitation extremes in a doubled CO₂ (2XCO₂) and geoengineered climate (Geo-Engg) relative to the 1XCO₂ case. The changes in precipitation means in a geoengineered climate have been discussed in several previous studies^{8,15–18,41–43}. In the 2XCO₂ case, we found that the change in mean surface

temperature was 4.1 K and mean precipitation was 0.24 mm/day (7.9%). However, in the Geo-Engg case, the change in global mean temperature reduced to –0.07 K and precipitation to –0.08 mm/day (–2.8%).

Evaluation of model-simulated precipitation extremes

For evaluation of precipitation extreme statistics from the model, we used 99.9th percentile precipitation rates as the metric for comparison. As we are interested in the statistics of extremes, we have evaluated the spatial statistics of this quantity. Figure 1 shows the 99.9th percentile precipitation rates in control simulation (the 1XCO₂ case) and observational data (GPCP). Spatial statistics of the 1XCO₂ case and GPCP were compared over large domains and Giorgi land regions to evaluate the model-simulated extremes. It is evident from Figure 1 that the model-simulated spatial statistics is similar to that of observations over all large domains, except tropical and subtropical land regions, where the model slightly underestimates the extremes. Figure 2 shows the distribution of 99.9th percentile precipitation rates around the globe. The distribution of global daily precipitation rates (Figure 3) and extreme (in this case, 99.9th percentile) precipitation rates (Figure 2) shows different characteristics. The probability density function (PDF) of daily precipitation rates is skewed towards right compared to that for precipitation extremes (Figure 3). It can be seen from Figure 2 that PDF of GPCP data is slightly shifted towards right compared to the 1XCO₂ case, showing that the model slightly underestimates precipitation extremes. However, the model overestimates precipitation rates for precipitation extremes less than 40 mm/day.

We also evaluated the model-simulated precipitation extremes using bias and correlation coefficient over spatial pattern (Figure 4). We found that the model-simulated intensity of precipitation extremes showed almost similar spatial pattern (correlation coefficient for 99.9p was 0.66 and for RX5day was 0.69) to that in GPCP observational data (for the period 2004–2013). The mean biases were 5.6 and 3.4 mm/5 days for 99.9p and RX5day indices respectively. The model underestimated

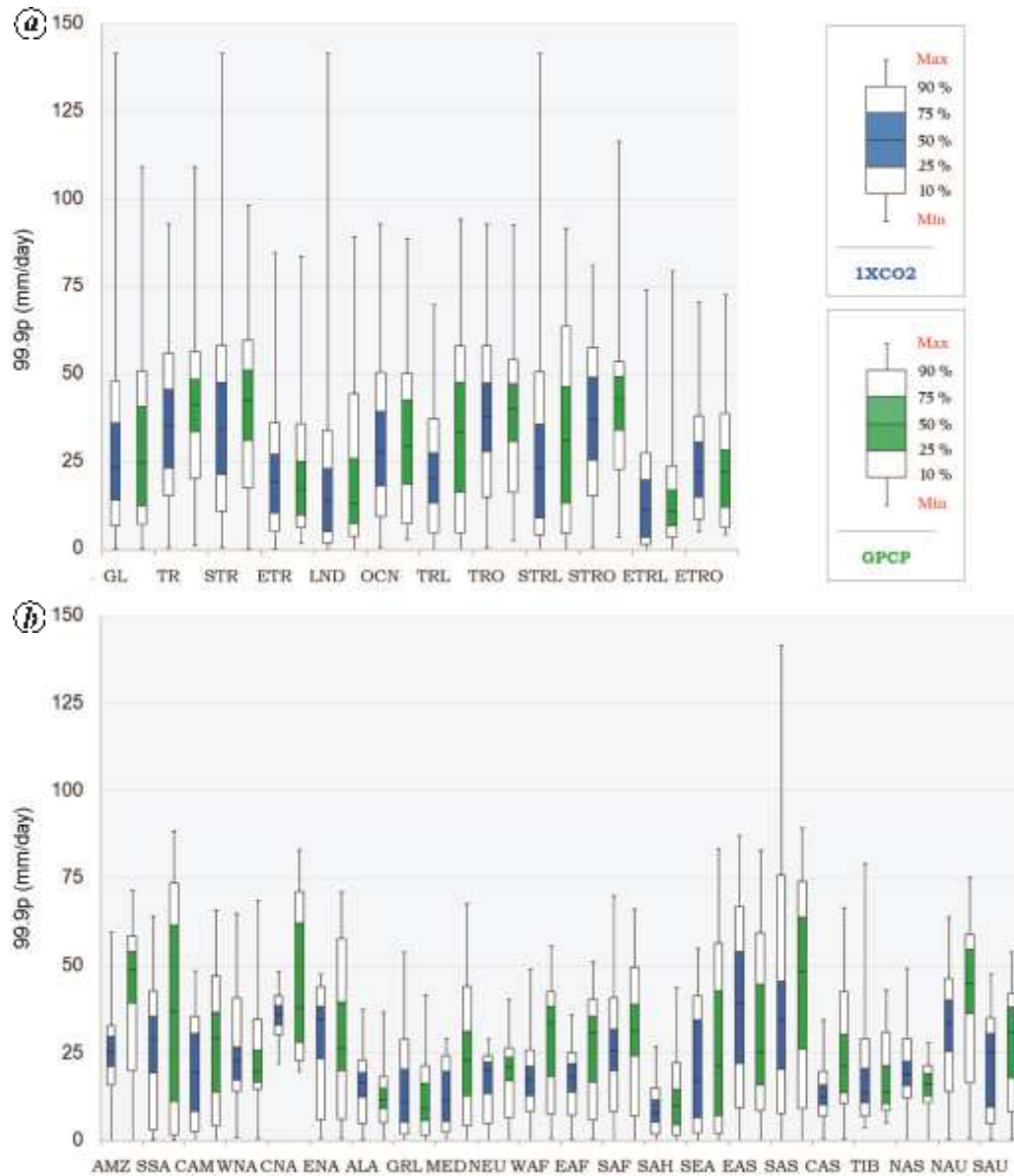


Figure 1. Comparison of the 99.9th percentile extreme precipitation rate (99.9p) of control simulation (1XCO₂; blue) with observational data (GPCP; green) for (a) large domains and (b) 22 Giorgi land regions.

the precipitation extremes over low- and mid-latitude land regions (Figure 4). However, the frequency of precipitation extremes (R20mm) showed a reduced correlation coefficient of 0.42 only. The mean bias in this index was 2.1 days.

Changes in intensity of precipitation extremes

The PDF of daily precipitation intensity was non-Gaussian and skewed (Figure 4) towards right. All the three experiments followed the same PDF, except for the heavy precipitation events (>50 mm/day)³⁷. It is known that in a skewed distribution such as that of precipitation, a change in the mean of the distribution generally affects its variability or spread and thus an increase in mean pre-

cipitation would also imply an increase in heavy precipitation events, and vice versa⁴⁴. Also, changes in tails have direct implications for occurrence of extreme events. The intensity of the extreme events (>50 mm/day) increased in the 2XCO₂ case relative to the 1XCO₂ case (inset, Figure 3). The mean and variance of precipitation distribution increased strongly (mean = 3.03 mm/day and standard deviation = 0.0087 mm/day for the 1XCO₂ case; mean = 3.28 mm/day and standard deviation = 0.0097 mm/day for the 2XCO₂ case), as a result of which precipitation extremes were more prevalent in the 2XCO₂ case. It is evident from Figure 2 that in the 2XCO₂ case, the PDF of extremes is shifted towards right, implying increase in extreme (99.9th percentile) precipitation rate over the globe.

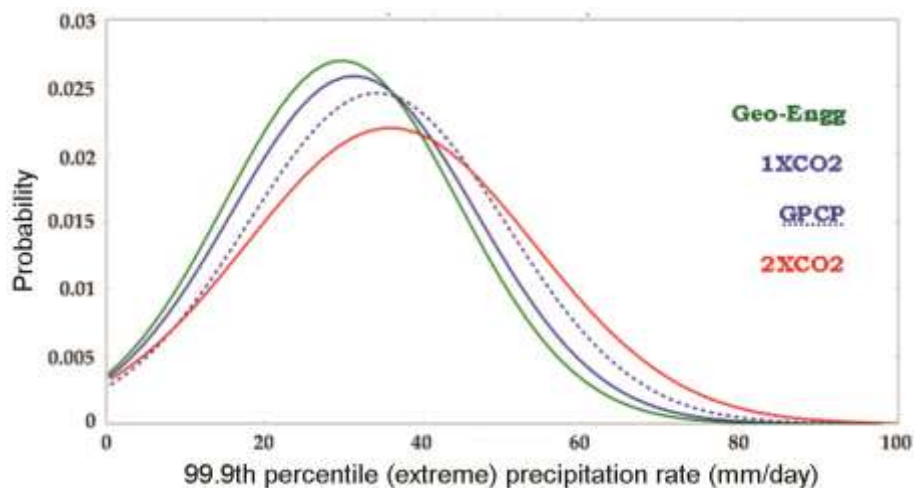


Figure 2. Probability density functions (over space) of extreme precipitation rates (99.9th percentile) for a 10-year period (91–100 years of daily output from simulations) of three experiments performed, i.e. 1XCO2 in blue, 2XCO2 in red, Geo-Engg in green and observational data (2004–13), i.e. GPCP in dashed blue line. The 99.9th percentile precipitation rates are estimated as explained in the text at every grid point over the 10-year period.

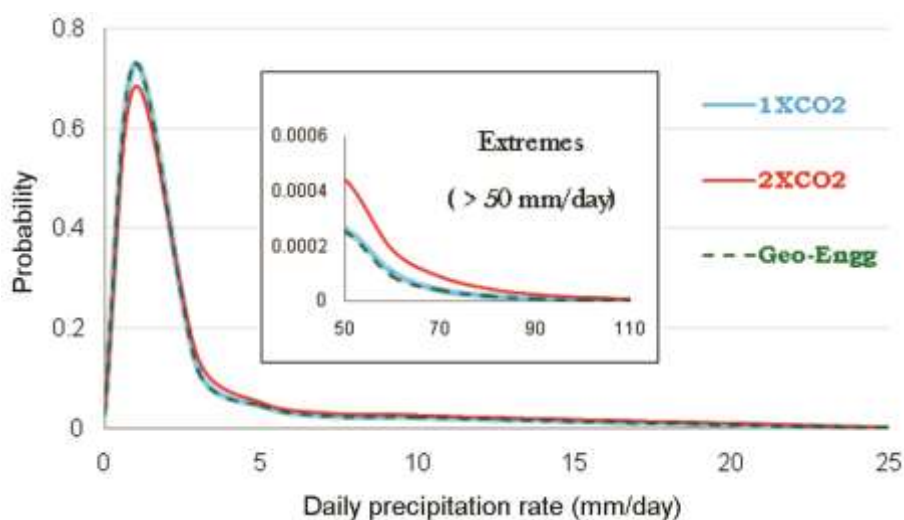


Figure 3. Comparison of daily precipitation PDFs of the three simulations, i.e. 1XCO2, 2XCO2 and Geo-Engg. (Inset) The extremes (>50 mm/day)³⁷ from the same PDFs are highlighted.

However, in the geoengineering simulation, intensity of the extremes was similar to the 1XCO2 case as shown by Curry *et al.*³⁰. The mean and variance in geoengineering were closer to that of the 1XCO2 case (mean = 2.96 mm/day and standard deviation = 0.0088 mm/day for Geo-Engg). Figure 2 also indicates that the extremes in the Geo-Engg case are brought close to the 1XCO2 case though the PDFs are not exactly identical in the two cases: extremes are reduced relative to the 1XCO2 case and moderate precipitation events (<40 mm/day) are increased in geoengineering simulation. The tails of PDFs differ between land and ocean regions ([Supplementary Figure 1](#)). A disproportionate reduction of evaporation over land compared to ocean in geoengineered climate is

likely to cause the different tails of precipitation PDFs, with oceans areas showing a reduction in extremes in the Geo-Engg case¹⁷.

We analysed the intensity of precipitation extremes using the three indices 99.9p, RX1day and RX5day. These indices were estimated over every grid point and therefore the threshold of extreme precipitation events was different for each grid point. We found that the changes in 99.9p were above the interannual variability (as the signal was larger than noise) than the other two indices ([Supplementary Figure 2](#)). The changes in RX1day and RX5day are generally small and within the interannual variability ([Supplementary Figure 2](#)). There is an increase in 99.9p by 17.7% in the 2XCO2 case and a

decrease by 3.8% in the Geo-Engg case relative to the 1XCO₂ case on a global basis. In the 2XCO₂ case, we found large increase in intensity of precipitation extremes over extra-tropical regions and reduction in tropical oceans ([Supplementary Figure 2](#)). These results are in agreement with many previous studies^{17,28,30}. We found similar changes in the global mean RX1day and RX5day indices of about 21–25% and –1.6% in the 2XCO₂ and Geo-Engg cases respectively. Though changes in RX1day and RX5day have spatial patterns similar to 99.9p, the magnitude of changes is greater than 99.9p but within the interannual variability ([Supplementary Figure 2](#)). On a regional scale, it is evident that the medians of change are close to zero in the Geo-Engg case and the length of whiskers (variability over the domain) is also reduced to a large extent when compared to the 2XCO₂ case (Figure 5). This suggests that barring some exceptions, extremes are reduced to a large extent in the Geo-Engg case when compared to the 2XCO₂ case ([Supplementary Figure 3](#)). Further, [Supplementary Figure 2](#) shows that though globally there is a reduction, northern high-latitude land regions show increase in extreme precipitation events in the Geo-Engg case compared to the 1XCO₂ case.

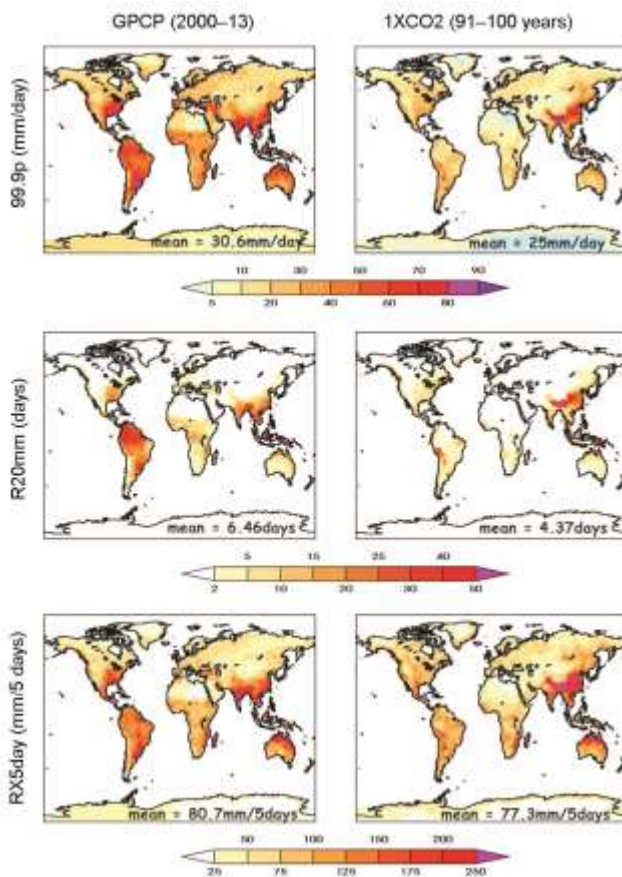


Figure 4. Spatial pattern of precipitation extreme indices 99.9p (top panels), R20mm (middle panels) and RX5day (bottom panels; description of the indices is given in Table 1) for GPCP (observational data for 2004–13, left panels) and the 1XCO₂ case (control simulation for 91–100 years, right panels).

Changes in frequency of precipitation extremes

We analysed the frequency of precipitation extremes using the three indices R1mm, R20mm and R50mm (Table 1). We found that as the threshold level increased, there was reduction in the changes in frequency of extreme precipitation events; they were mostly within the interannual variability ([Supplementary Figure 4](#)). There was global mean increase in number of wet days (R1mm) by 4.4 days in the 2XCO₂ case and a decrease by 3.6 days in the Geo-Engg case with relative to the 1XCO₂ case ([Supplementary Figure 4](#)). In the 2XCO₂ case, we found an increase in frequency of precipitation extremes over all the large domains except tropical and subtropical oceans where both increases and decreases were observed ([Supplementary Figure 4](#)). Changes in the number of very heavy precipitation days (R20mm) and extreme precipitation days (R50mm) were very small (Figure 6) and mostly within interannual variability at several locations ([Supplementary Figure 4](#)). However, we simulated a large increase of around 15–25 and 3–5 days in R20mm and R50mm respectively, along the coast of western Pacific and southeast Asian region ([Supplementary Figure 4](#)). In the Geo-Engg case, we found reduction in frequency of wet days (R1mm) all over the globe, but with a slight increase along the Inter-Tropical Convergence Zone (ITCZ). The large increase of R20mm and R50mm in the 2XCO₂ case over western Pacific and southeast Asia was offset in the Geo-Engg case, but slight positive changes remained ([Supplementary Figure 4](#)). On the regional scale, the number of wet days (R1mm) had reduced in the Geo-Engg case compared to the 2XCO₂ case (Figure 6), but frequencies of R20mm and R50mm events were similar to those in the 1XCO₂ case.

Changes in zonal mean intensity and frequency of precipitation extremes

Zonal means of extremes (99.9p and R20mm representing intensity and frequency of precipitation extremes respectively) showed that in the 2XCO₂ case zonal mean of both intensity and frequency of extremes was larger than that in the 1XCO₂ case all over the globe by around 5–10% in 99.9p and 2–3 days in R20mm (Figure 7). In contrast, the Geo-Engg case had reduced zonal mean extremes (both 99.9p and R20mm) than that in the 1XCO₂ case. The reduction in extremes was prominent over the southern tropical region (Figure 7). This large reduction of extremes over tropical ocean in the Geo-Engg case can be explained by a reduction in mean surface temperature in that region. We simulated a cooling of about 0.5 K (in surface mean temperature) in the Geo-Engg case over the tropical ocean resulting in smaller precipitation means and extremes in those regions. This tropical cooling in the Geo-Engg case relative to the 1XCO₂ case is a robust

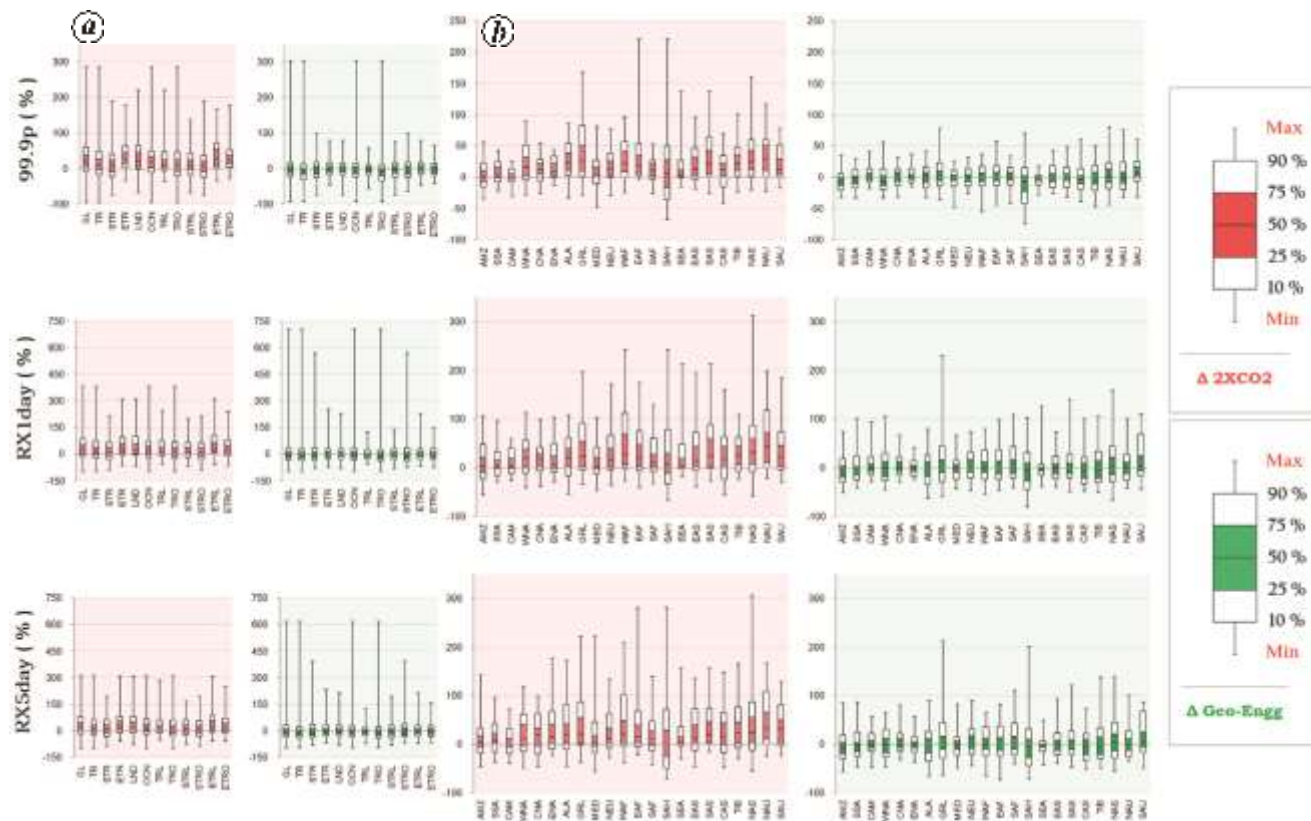


Figure 5. Change in intensity of precipitation extremes in the 2XCO2 (red) and Geo-Engg (green) cases relative to the 1XCO2 case, represented using the three indices 99.9p (extremely wet days; top panels), RX1day (maximum 1 day precipitation; middle panels) and RX5day (maximum 5 days precipitation; bottom panels; description of the indices is given in Table 1). The percentage changes in 99.9p, RX1day and RX5day are shown on regional scales, i.e. box whisker plot over (a) large domains and (b) 22 Giorgi land regions. Spatial statistics over the corresponding domains in the form of box with quartile ranges of 90%, 75%, 50%, 25% and 10% is also shown in the index on the right. The maximum and minimum changes over the domain are represented by whiskers at the top and bottom.

feature, as shown by several previous studies^{10,15–17,43,45,46}. In summary, we found that the CO₂ induced zonal mean extremes (99.9p and R20mm) were nearly brought back to pre-industrial climatic conditions by geoengineering, except over the tropical oceanic region where there was significant reduction.

Comparison of changes in precipitation means and extremes

As the surface warms up in the 2XCO2 case relative to the 1XCO2 case, both means and extremes change, but at different rates^{20,34,37}. We used 99.9p to represent the extremes for comparison with means. In the 2XCO2 case, we found that the extreme precipitation changed at a rate which was almost twice that of change in mean precipitation all over the globe, with an exception in the extra tropical land region where the rates of change were similar for both means and extremes (Figure 8). While global mean precipitation increased by 7.78% for a doubling of CO₂, the extremes increased by 17.7%. In the tropical land we simulated maximum difference between change in mean precipitation (5%) and extreme precipitation

(20%) (Figure 8 a). In contrast, though the magnitude of changes was small, we again simulated vastly different changes in means and extremes in the Geo-Engg case. Tropical Ocean (TRO) showed the highest reduction in means (4.8%) and extremes (8.9%) (Figure 8 a). In the 2XCO2 case we simulated more increase in precipitation extremes than the means over the whole of Asia, Africa and Australia, with the largest difference between extreme precipitation change (22.5%) and mean precipitation change (3.5%) over the southeast Asian region (SEA). In the Geo-Engg case, we simulated more reduction in mean than the extremes over most land regions (Figure 8 b). Over a few regions such as Mexico (CAM) in both 2XCO2 and Geo-Engg cases, means had reduced whereas extremes increased. This may result in an increase in the frequency of both droughts and floods in those regions. Overall, we found that there are large regional disparities in the geoengineering simulations (Figure 8 b).

Discussion and conclusion

Here, we have analysed the precipitation extremes in a doubled CO₂ climate with (the Geo-Engg case) and without

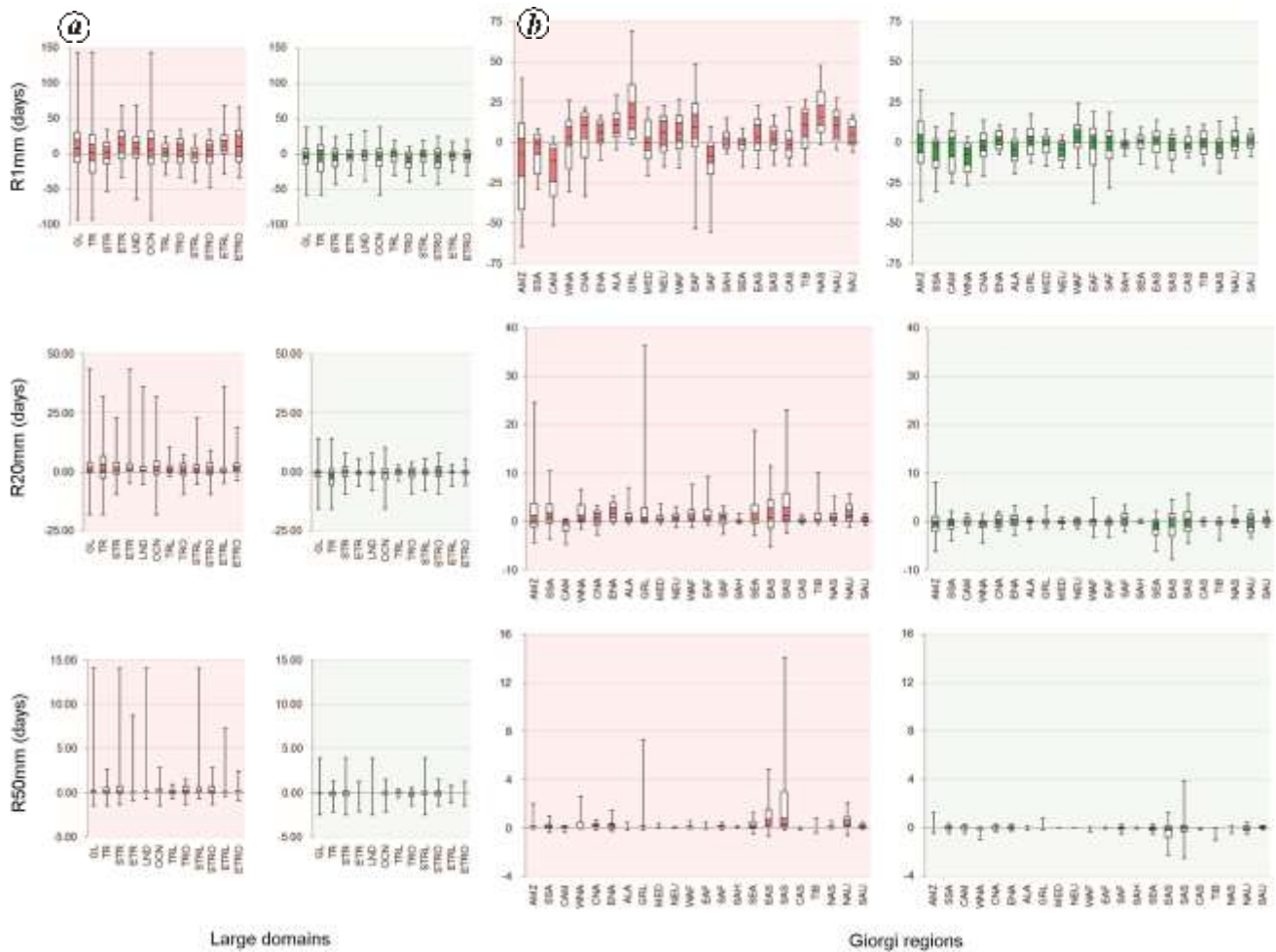


Figure 6. Same as in Figure 5, but for the change in frequency of precipitation extremes, represented using the three indices R1mm (number of wet days; top panels), R20mm (very heavy precipitation days; middle panels) and R50mm (extreme precipitation days; bottom panels; description of the indices is given in Table 1).

geoengineering (the 2XCO₂ case) and compared them with the 1XCO₂ case. Using a subset of precipitation extreme indices available in EIA and also some new indices appropriately defined for this study, we have performed a comprehensive analysis of precipitation extremes and discuss our results by segregating these into intensity-based and frequency-based indices. These indices were estimated at each grid point and averaged over corresponding domains of interest for a comprehensive analysis on a regional scale. Statistical analysis was performed over a few selected large domains and 22 Giorgi land regions.

In the 2XCO₂ case, we simulated an increase in global mean precipitation of $\sim 7.78\%$, and an increase in extreme precipitation of $\sim 17.7\%$ relative to the 1XCO₂ case. Intensity of precipitation extremes (RX1day and RX5day) increased by $\sim 20\%$ in the 2XCO₂ case. In the Geo-Engg case, the mean precipitation had slightly reduced relative to the 1XCO₂ case, although the mean surface temperature change was very small¹⁸. In agreement with previous

studies, intensity of precipitation extremes in the Geo-Engg case was brought close to the 1XCO₂ case globally, except over the tropical ocean where the extremes were less than those in the 1XCO₂ case. This reduction can be explained by the residual cooling over tropical oceans that occurs in geoengineered climate^{10,43,46}.

We simulated an increase in the global mean number of wet days (R1mm) by up to ~ 4.4 days in the 2XCO₂ case relative to the 1XCO₂ case. Similarly, we simulated an increase in the frequency of heavy (R20mm; ~ 20 days) and extreme (R50mm; ~ 5 days) precipitation events in the 2XCO₂ case. In the Geo-Engg case, the increase in the frequency of the heavy and extreme precipitation events due to CO₂ doubling was nearly offset. We simulated a decrease in the global mean number of wet days (R1mm) by ~ 3.6 days relative to the 1XCO₂ case. However, there are small residual changes simulated in the regions near ITCZ. We also analysed the zonal means of extremes (99.9p and R20mm) for both 2XCO₂ and Geo-Engg cases. We simulated an increase in the intensity

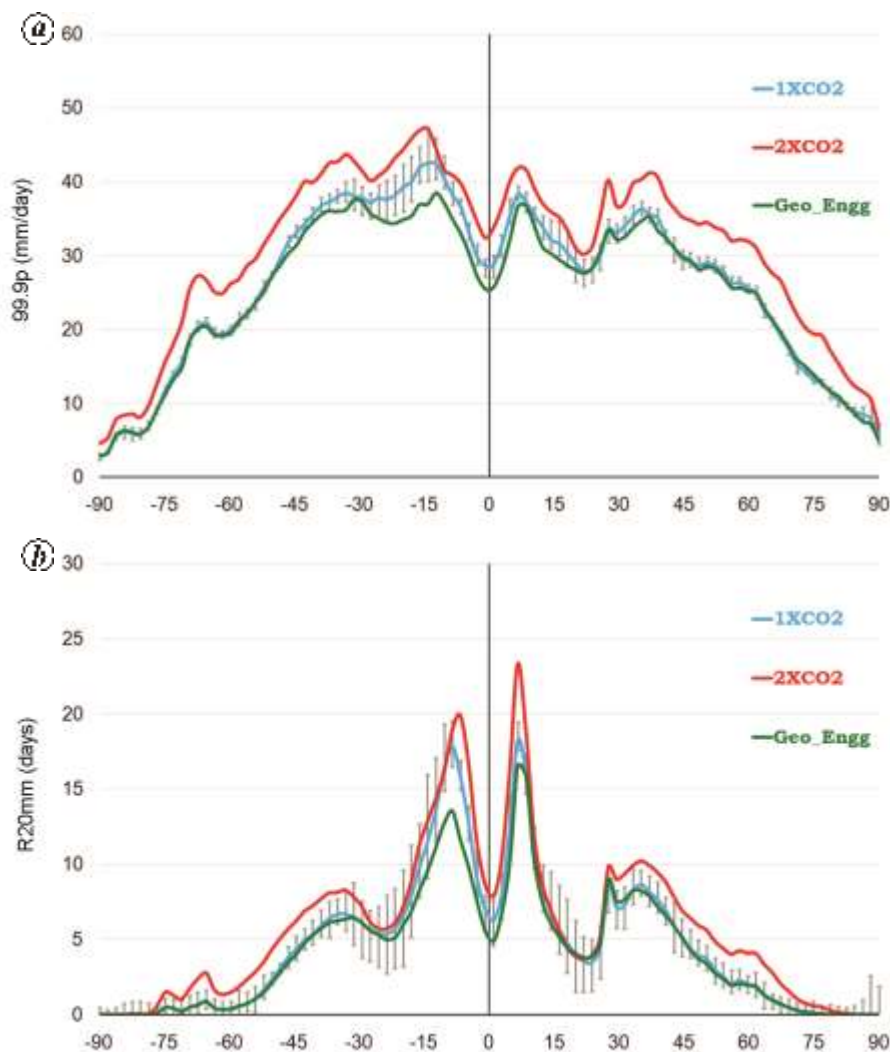


Figure 7. Zonal mean of (a) intensity of extreme precipitation (99.9p) and (b) frequency of extreme precipitation (R20mm) for the 10-year analysis period (91–100 years period in simulations performed) calculated for the control (1XCO₂; blue), doubled CO₂ (2XCO₂; red) and geoengineering (Geo-Engg; green) simulations. Grey bars represent the range of extremes in ten 5-year segments of the last 50-year data of the control simulation (1XCO₂).

(~5–10% in 99.9p) and frequency (~2–3 days in R20mm) all over the globe in the 2XCO₂ case relative to the 1XCO₂ case. However, in the Geo-Engg case, there was a net reduction in both intensity and frequency of precipitation extremes relative to the 1XCO₂ case. This reduction was more prominent in the tropical region, as there is a cooling of ~0.5 K simulated in the tropical ocean.

It is known that means and extremes vary due to different physical processes. While the mean precipitation is dependent on moisture content and global atmospheric circulation³⁷, the physical processes on which precipitation extremes are dependent, are an interesting topic for further in-depth study. Also, understanding the effects of these changes in climate extremes on evapotranspiration and vegetation on a regional scale could be important, but that is beyond the scope of this study.

There are several limitations to this study. Our simulations are idealized equilibrium experiments designed to demonstrate the effects of SRM geoengineering on extremes. The model-simulated precipitation extremes show some biases in the precipitation extremes over a few regions. Our model lacks deep ocean feedbacks and a dynamic sea-ice, and hence the ocean heat transport changes due to CO₂ increase and geoengineering, and the transient effects are not modelled realistically in our simulations. Our results are based on a single model. The robustness of our results can be assessed only if a similar analysis is performed using multiple models. Several previous studies performed such a multi-model analysis for geoengineered climate using GeoMIPdata^{17,30}. The reduction in precipitation extremes (such as RX 5 day precipitation amount) due to geoengineering relative to the pre-industrial climate has been discussed in previous

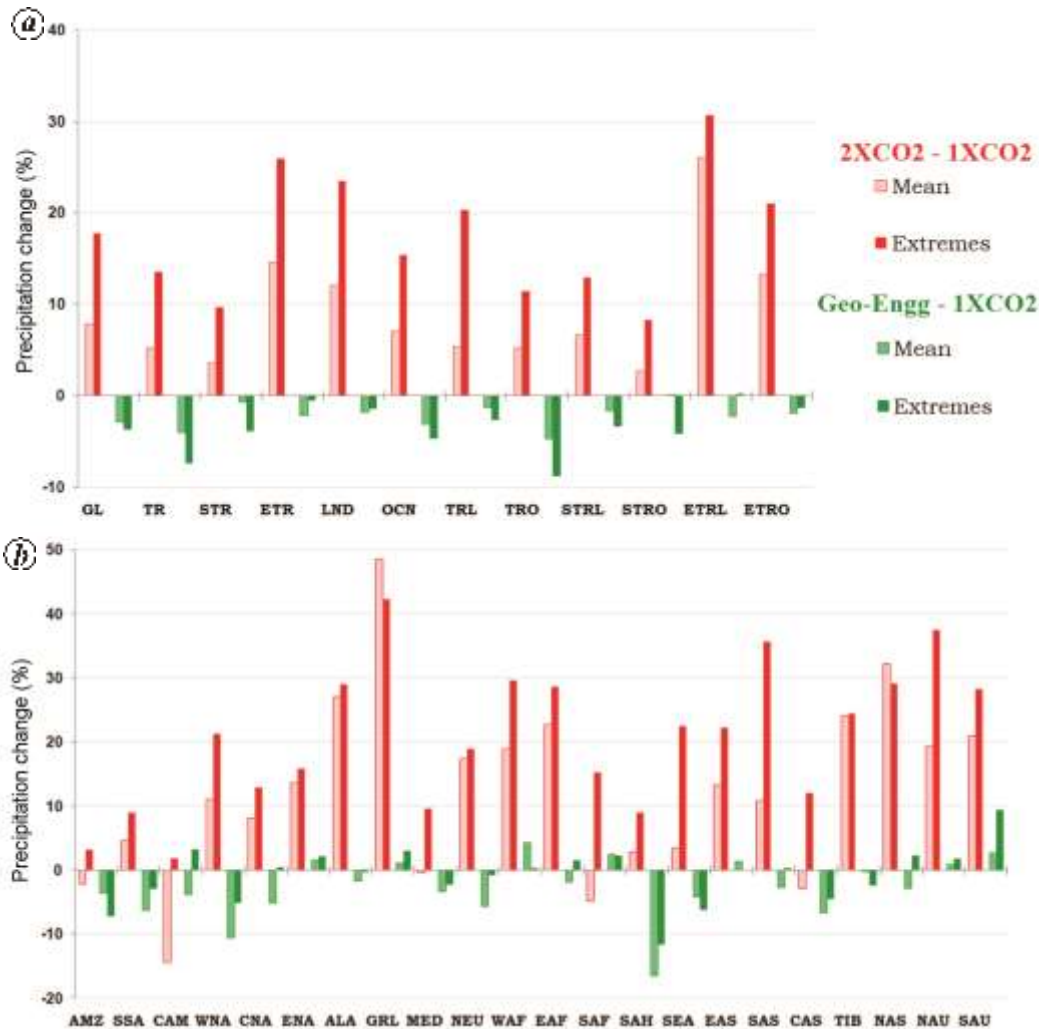


Figure 8. Change in precipitation means and extremes (99.9p) over (a) large domains and (b) 22 Giorgi land regions in the 2XCO₂ (red bars) and Geo-Engg (green bars) simulations relative to the 1XCO₂ simulation.

studies^{17,30}, and our results are qualitatively in agreement with these findings.

In this study, solar constant reduction was used to mimic geoengineering. It is not clear whether other SRM methods would show similar results. Several studies have recently compared the mean climate states produced by different SRM methods^{43,47–51}. For example, Kalidindi *et al.*⁴³ showed that the mean tropospheric climate change is similar for simulations with solar constant reductions and with equivalent stratospheric aerosols. However, none of these studies has compared extremes under different SRM schemes. In a study that focused on extreme analysis for geoengineered climate, two SRM geoengineering methods – marine cloud brightening and stratospheric sulphate injection were compared⁵². It was shown that stratospheric sulphate injection is effective in offsetting precipitation over land, whereas marine cloud brightening is effective over ocean. Because these two SRM geoengineering methods showed different extreme precipitation changes⁵² when compared to our results, we

suggest multi-model studies on the effects of various other SRM geoengineering methods.

In conclusion, geoengineering can potentially offset the increase in both intensity and frequency of precipitation extremes caused by CO₂-induced climate change. However, there are large residual changes in the mean and extreme precipitation on a regional scale.

1. IPCC, Contribution of Working Group I to the fifth assessment report of the Intergovernmental Panel on Climate Change. In *Climate Change 2013: The Physical Science Basis* (eds Stocker, T. F. *et al.*), Cambridge University Press, Cambridge, UK, 2013.
2. Keith, D. W., Geoengineering the climate: history and prospect. *Annu. Rev. Energ. Environ.*, 2000, **25**, 245–284; doi:10.1146/annurev.energy.25.1.245.
3. Bala, G., Problems with geoengineering schemes to combat climate change. *Curr. Sci.*, 2009, **96**(1), 42–48.
4. Shephard *et al.*, Geoengineering the climate: science, governance and uncertainty. The Royal Society, London, 2009; https://royalsociety.org/~media/Royal_Society_Content/policy/publications/2009/8693.pdf (accessed on 19 June 2015).

5. Vaughan, N. E. and Lenton, T. M., A review of climate geoengineering proposals. *Climate Change*, 2011, **109**, 745–790; doi:10.1007/s10584-011-0027-7.
6. Caldeira, K., Bala, G. and Cao, L., The science of geoengineering. *Annu. Rev. Earth Planet. Sci.*, 2013, **41**, 231–256; doi:10.1146/annurev-earth-042711-105548.
7. NAS, Climate intervention: reflecting sunlight to cool earth. National Academy of Sciences Report, National Academies Press, USA, 2015; <https://nas-sites.org/americasclimatechoices/other-reports-on-climate-change/2015-2/climate-intervention-reports/> (accessed on 19 June 2015).
8. Govindasamy, B. and Caldeira, K., Geoengineering earth's radiation balance to mitigate CO₂-induced climate change. *Geophys. Res. Lett.*, 2000, **27**, 2141–2144; doi:10.1029/1999GL006086.
9. Govindasamy, B., Thompson, S., Duffy, P. B., Caldeira, K. and Delire, C., Impact of geoengineering schemes on the terrestrial biosphere. *Geophys. Res. Lett.*, 2002, **29**(22), 2061; doi:10.1029/2002GL015911.
10. Govindasamy, B., Caldeira, K. and Duffy, P. B., Geoengineering earth's radiation balance to mitigate climate change from a quadrupling of CO₂. *Global Planet. Change*, 2003, **37**(1–2), 157–168; doi:10.1016/S0921-8181(02)00195-9.
11. Matthews, H. D. and Caldeira, K., Transient climate-carbon simulations of planetary geoengineering. *Proc. Natl. Acad. Sci. USA*, 2007, **104**, 9949–9954; doi:10.1073/pnas.0700419104.
12. Robock, A., Oman, L. and Stenchikov, G. L., Regional climate responses to geoengineering with tropical and arctic SO₂ injections. *J. Geophys. Res.*, 2008, **113**, D16101; doi:10.1029/2008JD010050.
13. Rasch, P. J. *et al.*, An overview of geoengineering of climate using stratospheric sulphate aerosols. *Philos. Trans. R. Soc. London, Ser. A*, 2008, **366**, 4007–4037; doi:10.1098/rsta.2008.013.
14. Ricke, K. L., Granger Morgan, M. and Allen, M. R., Regional climate response to solar radiation management. *Nature Geosci.*, 2010, **3**, 537–541; doi:10.1038/ngeo915.
15. Schmidt, H. *et al.*, Solar irradiance reduction to counteract radiative forcing from a quadrupling of CO₂: climate responses simulated by four earth system models. *Earth Syst. Dyn.*, 2012, **3**, 63–78; doi:10.5194/esd-3-63-2012.
16. Kravitz, B. *et al.*, Climate model response from the Geoengineering Model Intercomparison Project (GeoMIP). *J. Geophys. Res. Atmos.*, 2013, **118**, 8320–8331; doi:10.1002/jgrd.50646.
17. Tilmes, S. *et al.*, The hydrologic impact of Geoengineering in the Geoengineering Model Intercomparison Project (GeoMIP). *J. Geophys. Res. Atmos.*, 2013, **118**, 11036–11058; doi:10.1002/jgrd.50868.
18. Bala, G., Duffy, P. B. and Taylor, K. E., Impact of geoengineering schemes on the global hydrological cycle. *Proc. Natl. Acad. Sci. USA*, 2008, **105**, 7664–7669; doi:10.1073/pnas.0711648105.
19. Muthyala, R., Bala, G. and Nalam, A., Regional scale analysis of climate extremes in an SRM geoengineering simulation, Part 2: temperature extremes. *Curr. Sci.*, 2018, **114**(5), 1036–1045.
20. Kharin, V. V. and Zwiers, F. W., Estimating extremes in transient climate change simulations. *J. Climate*, 2005, **18**, 1156–1173.
21. Emori, S. and Brown, S., Dynamic and thermodynamic changes in mean and extreme precipitation under changed climate. *Geophys. Res. Lett.*, 2005, **32**, L17706; doi:10.1029/2005GL023272.
22. Held, I. M. and Soden, B. J., Robust responses of the hydrological cycle to global warming. *J. Climate*, 2006, **19**, 5686–5699; doi:10.1175/JCLI3990.1.
23. Barnett, D. N., Brown, S. J., Murphy, J. M., Sexton, D. M. H. and Webb, M. J., Quantifying uncertainty in changes in extreme event frequency in response to doubled CO₂ using a large ensemble of GCM simulations. *Climate Dyn.*, 2006, **26**, 489–511; doi:10.1007/s00382-005-0097-1.
24. Kharin, V. V., Zwiers, F. W., Zhang, X. and Hegerl, G. C., Changes in temperature and precipitation extremes in the IPCC ensemble of global coupled model simulations. *J. Climate*, 2007, **20**, 1419–1444; doi:10.1175/JCLI4066.1.
25. Allan, R. P. and Soden, B. J., Atmospheric warming and the amplification of precipitation extremes. *Science*, 2008, **321**, 1481–1484; doi:10.1126/science.1160787.
26. O'Gorman, P. A. and Schneider, T., Scaling of precipitation extremes over a wide range of climates simulated with an idealized GCM. *J. Climate*, 2009, **22**, 5676–5685.
27. Sillmann, J., Kharin, V. V., Zhang, X., Zwiers, F. W. and Bronaugh, D., Climate extreme indices in the CMIP5 multi-model ensemble: Part 1. Model evaluation in the present climate. *J. Geophys. Res. Atmos.*, 2013, **118**, 1716–1733; doi:10.1002/jgrd.50203.
28. Sillmann, J., Kharin, V. V., Zhang, X., Zwiers, F. W. and Bronaugh, D., Climate extreme indices in the CMIP5 multi-model ensemble: Part 2. Future climate projections. *J. Geophys. Res. Atmos.*, 2013, **118**, 2473–2493; doi:10.1002/jgrd.50188.
29. O'Gorman, P. A., Sensitivity of tropical precipitation extremes to climate change. *Nature Geosci.*, 2012, **5**(10), 697–700; doi:10.1038/ngeo1568.
30. Curry, C. L. *et al.*, A multimodel examination of climate extremes in an idealized geoengineering experiment. *J. Geophys. Res. Atmos.*, 2014, **119**, 3900–3923; doi:10.1002/2013JD020648.
31. Richard, B. N. *et al.*, Description of the NCAR community atmosphere model (CAM 5.0). NCAR Technical Note NCAR/TN-464 + STR, National Centre for Atmospheric Research, Boulder, CO, USA, 2012.
32. Collins, W. D. *et al.*, Description of the NCAR Community Atmosphere Model (CAM 3.0). NCAR Technical Note NCAR/TN-464 + STR, National Centre for Atmospheric Research, Boulder, CO, USA, 2004.
33. World Meteorological Organization, The global climate (2001–2010). A decade of climate extremes. Summary Report WMO No. 1119, 2013; http://library.wmo.int/pmb_ged/wmo_1119_en.pdf (assessed 19 June 2015).
34. Allen, M. R. and Ingram, W. J., Constraints on future changes in climate and the hydrologic cycle. *Nature*, 2002, **419**, 224–232; doi:10.1038/nature01092.
35. Sun, Y., Solomon, S., Dai, A. and Portmann, R. W., How often will it rain? *J. Climate*, 2007, **20**, 4801–4818; doi:10.1029/2008GL036728.
36. O'Gorman, P. A. and Schneider, T., The hydrological cycle over a wide range of climates simulated with an idealized GCM. *J. Climate*, 2008, **21**, 3815–3832; doi:10.1175/2007JCLI2065.1.
37. Trenberth, K. E., Precipitation in a changing climate – more floods and droughts in the future. *GEWEX News*, 2009, **19**, 8–10.
38. Huffman, G. J. and Bolvin, D. T., Version 1.2: GPCP one-degree daily precipitation data set documentation. Mesoscale Atmospheric Processes Laboratory, NASA Goddard Space Flight Center and Science Systems and Applications, USA, 2013; ftp://meso.gsfc.nasa.gov/pub/idd-v1.2/IDD_V1.2_doc.pdf (accessed on 19 June 2015).
39. Trenberth, K. E., Changes in precipitation with climate change. *Climate Res.*, 2011, **47**, 123–138; doi:10.3354/cr00953.
40. Giorgi, F. and Francisco, R., Uncertainties in regional climate change prediction: a regional analysis of ensemble simulations with the HadCM2 coupled AOGCM. *Climate Dyn.*, 2000, **16**, 169–182.
41. Bala, G., Caldeira, K., Nemani, R., Cao, L., Ban-Weiss, G. and Shin, H. J., Albedo enhancement of marine clouds to counteract global warming: impacts on the hydrological cycle. *Climate Dyn.*, 2010, **37**(5–6), 915–931; doi:10.1007/s00382-010-0868-1.
42. Bala, G. and Nag, B., Albedo enhancement over land to counteract global warming: impacts on hydrological cycle. *Climate Dyn.*, 2012, **39**, 1527–1542; doi:10.1007/s00382-011-1256-1.
43. Kalidindi, S., Bala, G., Modak, A. and Caldeira, K., Modeling of solar radiation management: a comparison of simulations using

- reduced solar constant and stratospheric sulphate aerosols. *Climate Dyn.*, 2015, **44**, 2909–2925; doi:10.1007/s00382-014-2240-3.
44. Zhang, X. and Zwiers, F., Statistical indices for diagnosing and detecting changes in extremes. In *Extremes in a Changing Climate: Detection, Analysis and Uncertainty* (eds Agha Kouchak, A. et al.), Springer Science + Business Media, Heidelberg, Germany, 2012, pp. 1–14.
45. Lunt, D. J., Ridgwell, A., Valdes, P. J. and Seale, A., Sunshade world: a fully coupled GCM evaluation of the climatic impacts of geoengineering. *Geophys. Res. Lett.*, 2008, **35**, L12710; doi:10.1029/2008GL033674.
46. Modak, A. and Bala, G., Sensitivity of simulated climate to latitudinal distribution of solar insolation reduction in solar radiation management. *Atmos. Chem. Phys.*, 2014, **14**, 7769–7779; doi:10.5194/acp-14-7769-2014.
47. Ammann, C. M., Washington, W. M., Meehl, G. A., Buja, L. and Teng, H., Climate engineering through artificial enhancement of natural forcings: magnitudes and implied consequences. *J. Geophys. Res.*, 2010, **115**, D22109; doi:10.1029/2009JD012878.
48. Jones, A., Haywood, J. and Boucher, O., A comparison of the climate impacts of geoengineering by stratospheric SO₂ injection and by brightening of marine stratocumulus cloud. *Atmos. Sci. Lett.*, 2011, **12**, 176–183; doi:10.1002/asl.29.
49. Fyfe, J., Cole, J., Arora, V. and Scinocca, J., Biogeochemical carbon coupling influences global precipitation in geoengineering experiments. *Geophys. Res. Lett.*, 2013, **40**, 651–655; doi:10.1002/grl.50166.
50. Niemeier, U., Schmidt, H., Alterskjær, K. and Kristjánsson, J. E., Solar irradiance reduction via climate engineering: impact of different techniques on the energy balance and the hydrological cycle. *J. Geophys. Res. Atmos.*, 2013, **118**, 11; doi:10.1002/2013JD020445.
51. Ferraro, A. J., Highwood, E. J. and Charlton-Perez, A. J., Weakened tropical circulation and reduced precipitation in response to geoengineering. *Environ. Res. Lett.*, 2014, **9**, 014001; doi:10.1088/1748-9326/9/1/014001.
52. Aswathy, V. N., Boucher, O., Quaas, M., Niemier, U., Muri, H. and Quaas, J., Climate extremes in multi-model simulations of stratospheric aerosol and marine cloud brightening climate engineering. *Atmos. Chem. Phys. Discuss.*, 2014, **14**, 32393–32425; doi:10.5194/acpd-14-32393-2014.

ACKNOWLEDGEMENTS. This study was funded by the Divecha Centre for Climate Change, Indian Institute of Science (IISc), Bengaluru and the Department of Science and Technology (DST), New Delhi, (Grant DSTO1203). R.M. and A.N. acknowledge the scholarships provided by the Indian Institute of Science. Computations were carried out at the Centre for Atmospheric and Oceanic Sciences High Performance Computing facility funded by Fund for Improvement of S&T Infrastructure, DST and the Divecha Centre for Climate Change.

Received 30 August 2017; accepted 22 October 2017

doi: 10.18520/cs/v114/i05/1024-1035